ACS APPLIED MATERIALS & INTERFACES

Research Article

www.acsami.org

Multihydroxy Dendritic Upconversion Nanoparticles with Enhanced Water Dispersibility and Surface Functionality for Bioimaging

Li Zhou,* Benzhao He, Jiachang Huang, Zehong Cheng, Xu Xu, and Chun Wei

Guangxi Ministry-Province Jointly-Constructed Cultivation Base for State Key Laboratory of Processing for Nonferrous Metal and Featured Materials, Key Laboratory of New Processing Technology for Nonferrous Metal and Materials (Ministry of Education), and College of Material Science and Engineering, Guilin University of Technology, Guilin 541004, P. R. China

Supporting Information

ABSTRACT: Upconversion nanoparticle (UCNP) as a new class of imaging agent is gaining prominence because of its unique optical properties. An ideal UCNP for bioimaging should simultaneously possess fine water dispersibility and favorable functional groups. In this paper, we present a simple but effective method to the synthesis of a UCNP-based nanohybrid bearing a multihydroxy hyperbranched polyglycerol (HPG) shell by the combination of a "grafting from" strategy with a ring-opening polymerization technique. The structure and morphology of the resulting UCNP-*g*-HPG nanohybrid were characterized in detail by Fourier transform infrared, ^{1}H NMR, thermogravimetric analysis, and transmission electron microscopy measurements. The results reveal that the amount of grafted HPG associated with the thickness of the HPG shell can be well tuned. UCNP-*g*-HPG shows high water dispersibility and strong and stable upconversion luminescence. On the basis of its numerous surface hydroxyl groups, UCNP-*g*-HPG can be tailored by a representative fluorescent dye rhodamine B to afford a UCNP-*g*-HPG-RB nanohybrid that simultaneously presents upconversion and downconversion luminescence. Preliminary biological studies demonstrate that UCNP-*g*-HPG shows low cytotoxicity, high luminescent contrast, and deep light penetration depth, posing promising potential for bioimaging applications.

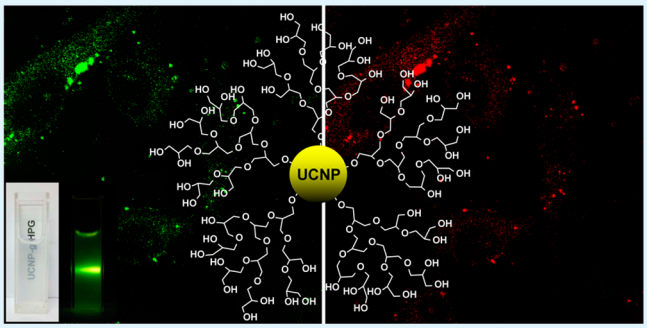

KEYWORDS: *upconversion nanoparticle, hyperbranched polyglycerol, water dispersibility, surface functionality, bioimaging*

1. INTRODUCTION

Lanthanide (Ln)-doped upconversion nanoparticle (UCNP), an emerging new class of luminescent nanomaterial, has shown tremendous potential in labelling biological entities because of its fascinating attributes, such as narrow emission peak, absence of photodamage, high photostability, deep light penetration depth, very low autofluorescence background, and low toxicity.[1−6] To facilitate the imaging applications, an ideal UCNP should simultaneously possess high water dispersibility and favorable surface functional groups for further coupling.[7−9]

Generally, a water-dispersible UCNP can be achieved by two strategies. One is to tailor the hydrophobic UCNP by employing ligand exchange,[10−12] ligand oxidation,[13] ligand capping,[14−16] surface silanization,[17,18] host−guest self-assembly,[19] and layer-by-layer (LBL) assembly[20] techniques for the introduction of hydrophilic components on the surface of a UCNP. An alternative strategy is to directly synthesize a water-dispersible UCNP by using hydrophilic polymers [e.g., poly(ethylenimine),[21,22] poly(vinylpyrrolidone),[22−24] poly(acrylic acid),[23] and poly(ethylene glycol)[23]] or small molecules (e.g., 6-aminohexanoic acid)[25,26] as ligands. For both of the strategies, surface engineering of UCNPs with polymers to form nanohybrids is a simple and effective approach.[20−28] The polymers can not only enhance the physical properties of the UCNP such as water dispersibility and processability but also endow the UCNP with numerous reactive functional groups and good biocompatibility. Although a number of polymers have been utilized to functionalize UCNPs, most polymers have no functional groups or only possess charged functional groups that may cause nonspecific interactions with biosubstrates during imaging applications. Therefore, exploring a method to functionalization of UCNPs with polymer ligands that contain multiple neutral functional groups (e.g., hydroxyl groups) is desired.

Another key point for UCNP/polymer nanohybrids is the thickness of the polymer shell on the surface of the UCNP. A too thin polymer shell associated with very low polymer content may not be able to impart sufficient desired properties to the UCNP, while an excessively thick polymer shell may result in the formation of a nanohybrid with extremely large size, which would cause an adverse impact on the imaging application. It is difficult to control the thickness of the polymer shell by the reported approaches (e.g., ligand exchange, ligand capping, and direct synthesis of UCNPs using polymers as

Received: February 18, 2014
Accepted: April 21, 2014
Published: April 21, 2014

   dx.doi.org/10.1021/am500980z | ACS Appl. Mater. Interfaces 2014, 6, 7719−7727

Scheme 1. Synthetic Route to UCNP-*g*-HPG and Modification of the Grafted HPG with Fluorescent Dye RhB

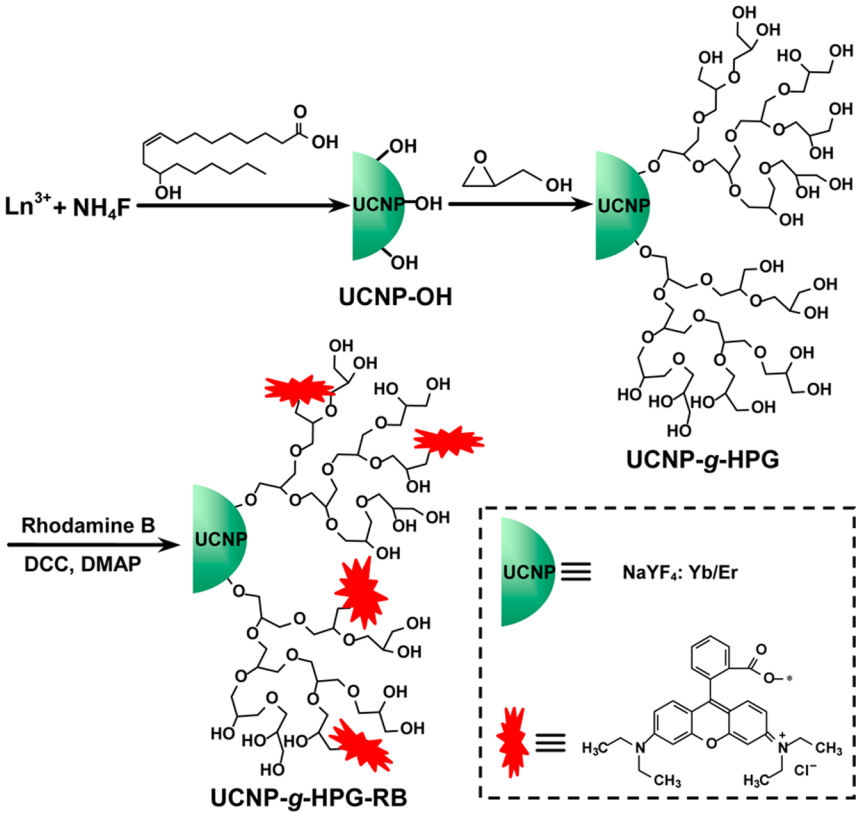

ligands) except for the LBL assembly technique, which can tune the thickness of the polymer shell by manipulating the number of repeated assemblies.[20,29] However, only charged polymers are suitable for this approach. To well control the thickness of the polymer shell, another promising approach is the direct growth of the desired polymer from the surface of the UCNP by using a surface-initiated living/controlled polymerization technique. This approach has been successfully employed to grow a polymer shell with controlled thickness on the surfaces of other inorganic nanoparticles (e.g., carbon nanotubes[30] and gold nanoparticles[31]). However, it has not been used to functionalize a UCNP, possibly because of the low availability of a UCNP with surface initiators.

In this paper, we report a novel water-dispersible $NaYF_4$:Yb/Er UCNP bearing a hyperbranched polyglycerol (HPG) shell by using surface-initiated anionic ring-opening polymerization (ROP; Scheme 1). As one of the most efficient host matrices for upconversion luminescence (UL),[32−35] $NaYF_4$ was chosen as the host material in this study. HPG was carefully chosen as the polymer shell because of its attractive merits such as high water solubility, excellent biocompatibility, and numerous hydroxyl groups.[36−40] Moreover, HPG can be synthesized with high controllability by a one-step reaction.[36,37] As expected, the combination of UCNP and HPG gives birth to a robust luminescent UCNP-*g*-HPG nanohybrid that shows attractive merits such as a tunable HPG shell, good water dispersibility, strong UL, low cytotoxicity, and versatile surface functionality, which highlight the potential of UCNP-*g*-HPG for bioimaging applications.

2. EXPERIMENTAL SECTION

Materials. Rare-earth chlorides ($LnCl_3{\cdot}6H_2O$, where Ln = Y, Yb, Er), ricinoleic acid (RA), 1-octadecene, ammonium fluoride, glycidol, *N*,*N*′-dicyclohexylcarbodiimide (DCC), 4-(dimethylamino)pyridine (DMAP), and rhodamine B (RhB) were purchased from Aladdin Chemistry Co. Ltd. (Shanghai, China). A potassium methylate solution in methanol (25 wt %, Aldrich) was used as received. Glycidol and dioxane were distilled before use. All other chemicals were of analytical grade and were used as received without further purification. Milli-Q water (18.2 MΩ) was used for all experiments.

Characterization. Fourier transform infrared (FTIR) spectra were measured on a Thermo Nexus 470 FTIR spectrometer (KBr disk). Thermogravimetric analysis (TGA) was carried on a Netzsch STA 449C analyzer with a heating rate of 20 °C/min in a nitrogen flow. ^{1}H NMR measurements were conducted on a Varian Mercury Plus 400 MHz spectrometer. The molecular weight was measured by gel permeation chromatography (GPC; PE series 200), with polystyrene as the standard and 0.01 M LiBr/dimethylformamide (DMF) as the eluent at a flow rate of 1 mL/min. Powder X-ray diffraction (XRD) spectra were taken on a Holland PANalytical X-Pert PRO X-ray diffractometer with Cu Kα radiation. Transmission electron microscopy (TEM) images were recorded on a JEM-2100 F high-resolution transmission electron microscope at 200 kV. Samples were prepared by placing a drop of a dilute aqueous dispersion on the surface of a copper grid. Dynamic light scattering (DLS) and ζ potential measurements were performed in aqueous solution using a Malvern Zetasizer Nano ZS90 apparatus. Luminescence spectra were recorded on a Varian fluorescence spectrophotometer. UL spectra were measured using an external 0−1000 mW adjustable continuous-wave laser (980 nm, Beijing Hi-Tech Optoelectronic Co., China) as the excitation source, instead of the xenon source in the spectrophotometer. Absorption spectra were recorded on a UV-3600 UV−vis−near-IR (NIR) spectrophotometer (Shimadzu). Confocal laser scanning microscopy (CLSM) images were recorded on a Zeiss LSM 510 confocal laser scanning microscope (Jena, Germany) equipped with a 980 nm NIR laser with an output power of 500 mW. Quantitative data were expressed as mean ± standard deviation unless specifically described. *P* values <0.05 were considered to be statistically significant.

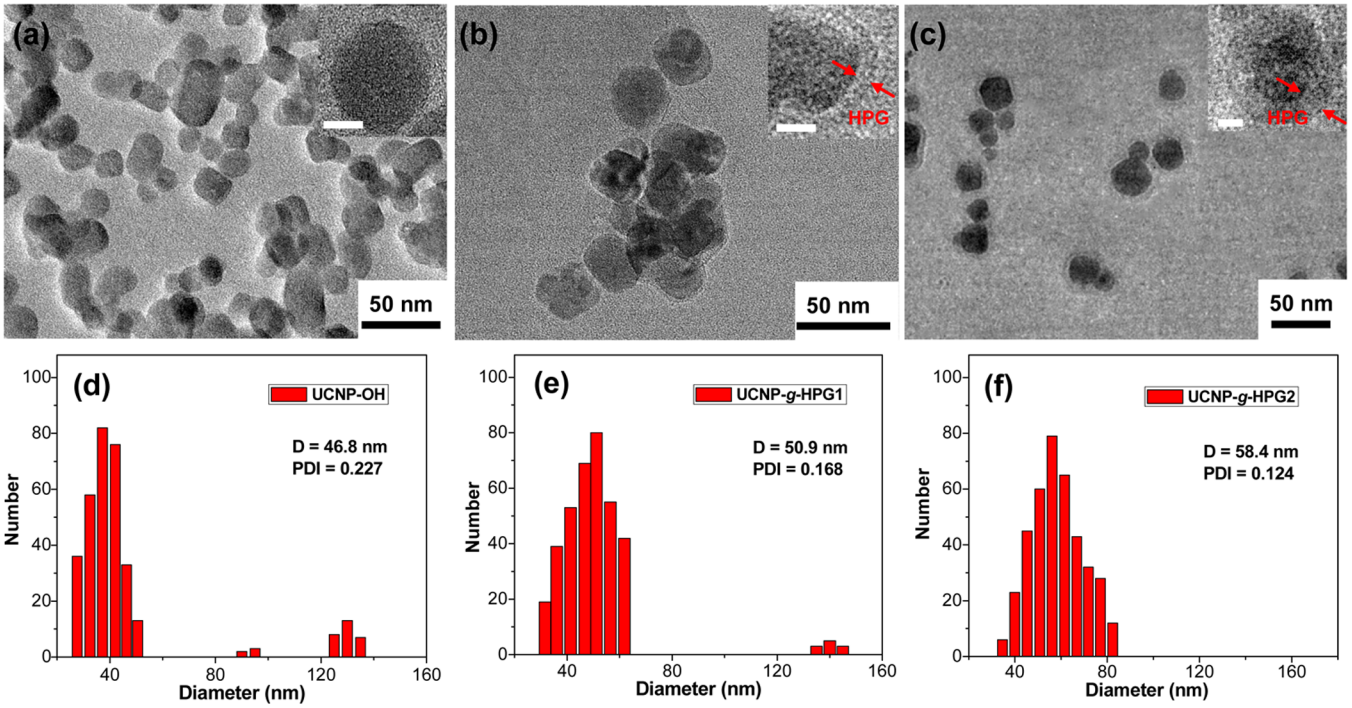

Figure 1. TEM images of (a) UCNP-OH, (b) UCNP-*g*-HPG1, and (c) UCNP-*g*-HPG2. The scale bar in the corresponding inset is 10 nm. Hydrodynamic radius distribution of (d) UCNP-OH, (e) UCNP-*g*-HPG1, and (f) UCNP-*g*-HPG2 at a concentration of 0.2 mg/mL.

Synthesis of UCNP-OH. In a typical procedure,[41] $YCl_3{\cdot}6H_2O$ (0.78 mmol), $YbCl_3{\cdot}6H_2O$ (0.2 mmol), and $ErCl_3{\cdot}6H_2O$ (0.02 mmol) were dissolved in 2 mL of water before 15 mL of RA and 15 mL of 1-octadecene were added in a 100 mL flask. The mixture was heated to 90 °C for 30 min and then vacuumed for another 30 min to form a transparent solution. Subsequently, the solution was cooled to room temperature and a methanol solution (12 mL) containing NaOH (100 mg, 2.5 mmol) and NH_4F (185 mg, 5 mmol) was added. The mixture was stirred for 15 min at room temperature, then transferred to a 100 mL autoclave, purged with argon for 5 min, sealed, and hydrothermally treated at 180 °C for 24 h. After the autoclave was cooled to room temperature naturally, the resulting product (designated as UCNP-OH) was separated by centrifugation, washed with ethanol, and dried at 60 °C for 12 h.

Synthesis of UCNP-*g*-HPG. UCNP-*g*-HPG was synthesized by an in situ ROP technique. Typically, UCNP-OH (80 mg) was mixed with 20 μL of a potassium methylate solution and 5 mL of anhydrous tetrahydrofuran in a flask. The mixture was stirred at 50 °C for 1 h before excess methanol was removed by a vacuum. A total of 10 mL of anhydrous dioxane was added, and the flask was placed in an ultrasonic bath for 15 min to ensure complete suspension of the UCNP-OH initiator. The mixture was heated to 95 °C, and a 20 wt % glycidol solution in dioxane was added dropwise over a period of 24 h. After completion of monomer addition, the mixture was stirred for an additional 6 h. After reaction, the mixture was quenched by methanol and subsequently centrifuged and washed several times with methanol. After repeated washing and centrifugation steps, the resulting solid product was dried overnight under vacuum at 50 °C. The weight feed ratios of glycidol monomer to UCNP-OH (R_{wt}) for UCNP-*g*-HPG1 and UCNP-*g*-HPG2 are 8.6:1 and 25.2:1, respectively. The corresponding free HPG was collected from the supernatant by precipitation with acetone.

Synthesis of UCNP-*g*-HPG-RB. Typically, 20 mg of UCNP-*g*-HPG2, 5 mg of RhB, and 10 mL of DMF were placed in a dry flask and treated in an ultrasonic bath for 3 min. Then, 18.6 mg of DCC and 5 mg of DMAP were added to the flask, and the mixture was stirred at 80 °C for 24 h. The product was separated by centrifugation and washed with ethanol repeatedly until the washed ethanol became colorless. After being dried overnight under vacuum, the product (designated as UCNP-*g*-HPG-RB) was obtained.

Cytotoxicity Evaluation. The cytotoxicity of the samples was examined using methylthiazolyldiphenyltetrazolium (MTT) assay. MCF-7 breast cancer cells were seeded in 96-well plates at a density of 4×10^4 cells/mL. After 24 h of incubation, the medium was replaced by the UCNP-*g*-HPG2 and UCNP-*g*-HPG-RB solutions with concentrations of 0, 0.1, 0.25, 0.5, and 0.8 mg/mL, respectively. The cells were then incubated for 24 h. After the designated time intervals, the wells were washed twice with 1 × PBS buffer. A total of 0.1 mL of a freshly prepared MTT (0.5 mg/mL) solution in a culture medium was added to each well. The MTT medium solution was carefully removed after 3 h of incubation. Dimethyl sulfoxide (DMSO; 100 μL) was then added into each well, and the plate was gently shaken for 10 min at room temperature to dissolve all of the precipitates. The absorbance of MTT at 570 nm was monitored by the microplate reader. The cell viability was expressed by the ratio of absorbance of the cells incubated with UCNP-*g*-HPG2 or UCNP-*g*-HPG-RB to that of the cells incubated with a culture medium only. Note that UCNP-*g*-HPG-RB shows weak absorption at 570 nm, and hence the real absorbance of cells incubated with UCNP-*g*-HPG-RB at 570 nm was calculated with the corresponding absorbance of a blank UCNP-*g*-HPG-RB solution as the reference.

Cell Imaging. MCF-7 cells were cultured in a RPMI 1640 medium containing 10% fetal bovine serum and 1% penicillin−streptomycin at 37 °C in a humidified environment of 5% CO_2. After 80% confluence, the medium was removed and the adherent cells were washed twice with 1 × PBS buffer. The UCNP-*g*-HPG solution (50 μg/mL, 0.4 mL) was then added to the chamber. After incubation for 2 h, cells were washed three times with 1 × PBS buffer and then fixed by 75% ethanol for 20 min, which was further washed twice with 1 × PBS buffer. The cells were imaged by a confocal laser scanning microscope (Nikon-A1) equipped with a 980 nm NIR laser and a Nikon digital camera.

In Vivo Animal Imaging. Animal procedures were in agreement with the guidelines of the Institutional Animal Care and Use Committee. UCNP-*g*-HPG-RB was dispersed in a PBS solution (pH 7.4) before imaging application. Kunming mice were anesthetized with ether. A total of 0.1 mL of UCNP-*g*-HPG-RB (50 μg/mL) was injected subcutaneously at the leg and bottom of the ear regions,

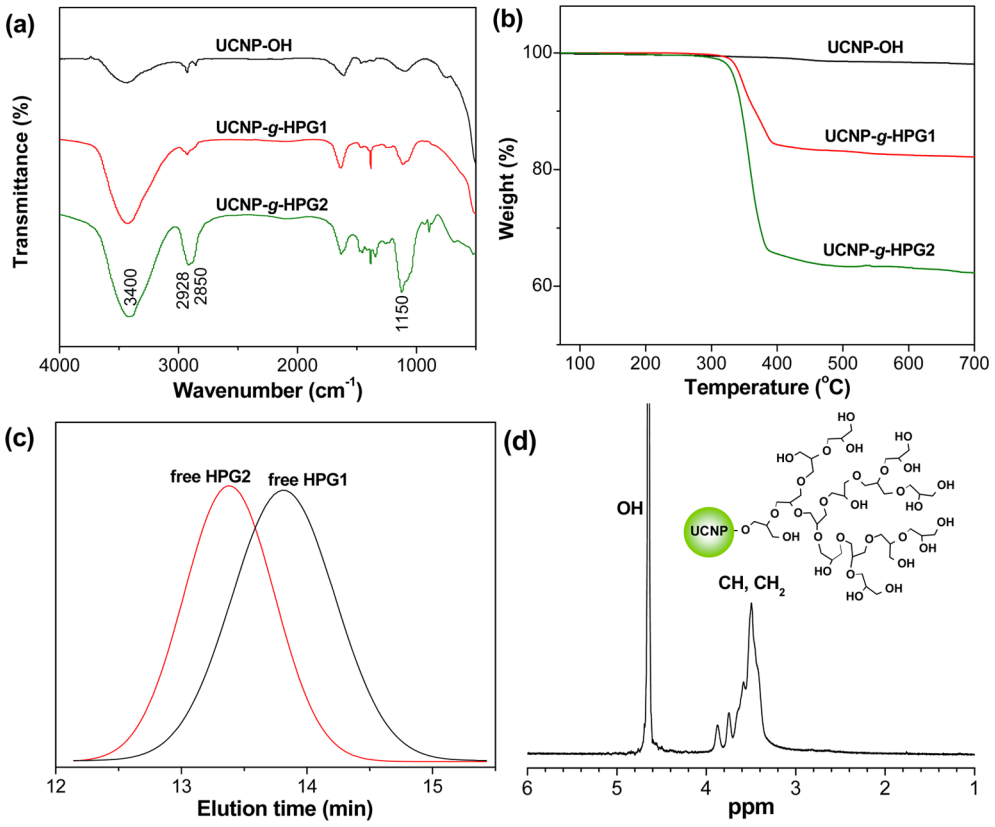

Figure 2. (a) FTIR spectra and (b) TGA curves of UCNP-OH, UCNP-*g*-HPG1. and UCNP-*g*-HPG2. (c) GPC curves of free HPG1 and free HPG2. (d) ^{1}H NMR spectrum of UCNP-*g*-HPG2 in D_2O.

respectively. The depth of injection was estimated from needle penetration. UL was observed in a darkened room under excitation of a 980 nm laser and recorded using a digital camera.

3. RESULTS AND DISCUSSION

Synthesis and Characterization. In order to graft HPG from the surface of the UCNP, a prerequisite is to obtain a UCNP with surface hydroxyl groups (UCNP-OH) that can initiate the ROP of the glycidol monomer.[36−38] Generally, the reported UCNPs have no functional groups or only possess charged amine or carboxylic groups.[6−9] Recently, we developed a one-step approach to synthesize UCNP-OH via a solvothermal technique by employing RA as the ligand.[41] TEM shows that the obtained UCNP-OH nanoparticles are generally spherical in shape with an average diameter of 25 ± 8 nm (Figure 1a). The crystalline structure of UCNP-OH was measured by powder XRD (Figure S1 in the Supporting Information, SI). The position and relative intensity of the diffraction peaks are in good agreement with the standard hexagonal phase structure of $NaYF_4$:Yb/Er (JCPDS 28-1192).[35,42] It should be noted that the $NaYF_4$:Yb/Er nanoparticles with hexagonal phase structure can exhibit much higher upconversion efficiency than their cubic phase counterpart.[35,42]

Table 1. Reaction Conditions and Selected Results for Grafting HPG from the Surface of the UCNP-OH

sample	R_{wt} [a]	f_{wt} (%) [b]	$M_{n,GPC}$ [c]	PDI [c]
UCNP-*g*-HPG1	8.6:1	17.5	5390	1.56
UCNP-*g*-HPG2	25.2:1	36.8	14230	1.48

[a]Weight feed ratio of glycidol monomer to UCNP-OH. [b]Weight fraction of grafted HPG calculated from the corresponding TGA data between 150 and 650 °C. [c]M_n and PDI of the corresponding free HPG.

In the FTIR spectrum of the UCNP-OH sample (Figure 2a), two obvious bands at 2850 and 2928 cm^{-1} associated with C−H stretching and two strong bands at 1150 and 3400 cm^{-1} respectively corresponding to C−O−C and −OH groups are observed, indicating that the RA ligands have been anchored onto the surface of the UCNP. The content of the organic moiety on the surface of the UCNP-OH was determined by TGA. The UCNP-OH sample shows a weight loss of 1.94 wt % between 150 and 650 °C (Figure 2b), confirming the presence of RA on the surface of the UCNP, and the corresponding density of the hydroxyl groups is ca. 0.065 mmol/g. Such a relatively high density of the initiator offers a good platform for the successful grafting of HPG. Although the presence of hydrophilic hydroxyl groups makes UCNP-OH water-dispersible, the formed aqueous dispersion is not stable enough and precipitation could be clearly observed after about 12 h because of the low content of the hydrophilic component on the surface of the UCNP-OH.

Growth of HPG on the surface of the UCNP-OH was realized by the combination of a "grafting from" strategy and a living ROP technique, as depicted in Scheme 1. The hydroxyl initiators of UCNP-OH were deprotonated by CH_3OK before the very slow addition of glycidol. Note that slow monomer addition is required for fine adjustment of the amount of grafted HPG because of the decrease of self-initiation of the glycidol monomer.[36,37] After polymerization, the resulting UCNP-*g*-HPG nanohybrid was washed repeatedly with water

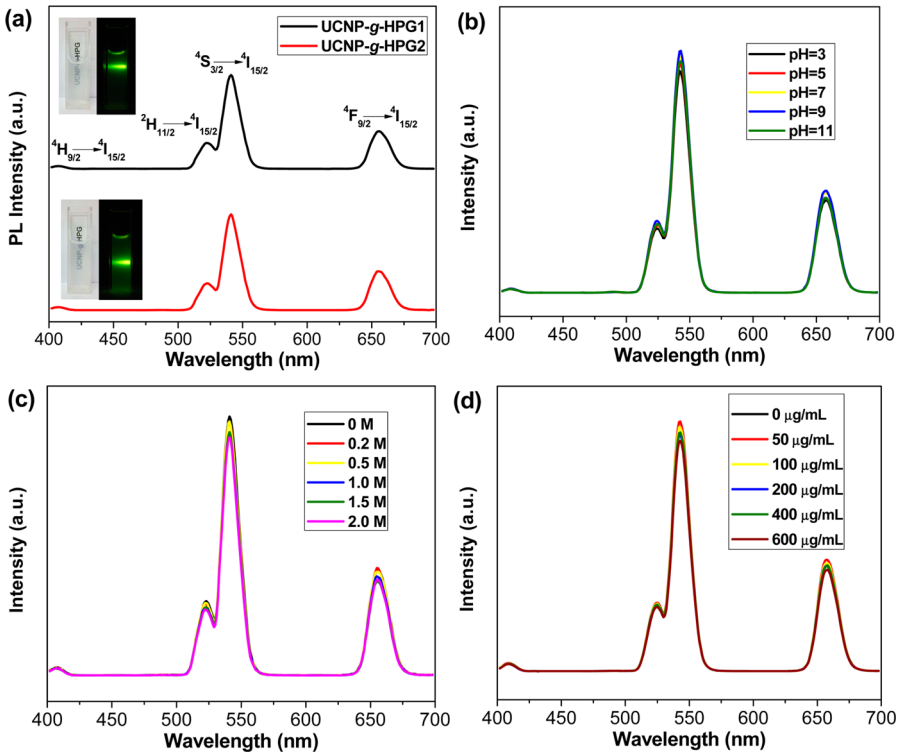

Figure 3. (a) Upconversion emission spectra (λ_{ex} = 980 nm) of UCNP-*g*-HPG1 and UCNP-*g*-HPG2. Inset: photographs of the corresponding samples in water (1 mg/mL) under daylight (left) and 980 nm laser illumination (right). (b) pH, (c) NaCl concentration, and (d) BSA concentration-dependent upconversion emission spectra of UCNP-*g*-HPG2 (1 mg/mL; λ_{ex} = 980 nm).

to remove ungrafted HPG (also called free HPG). In order to probe whether the amounts of grafted HPG can be tuned or not, several UCNP-*g*-HPG with different values of the weight feed ratio of glycidol to UCNP-OH (R_{wt}) were synthesized by keeping the other parameters constant (see Table 1). FTIR spectra of UCNP-*g*-HPG1 (R_{wt} = 8.6:1) and UCNP-*g*-HPG2 (R_{wt} = 25.2:1) show that the intensity of the absorption bands at 1150, 2850, 2928, and 3400 cm^{-1} are greatly enhanced compared with UCNP-OH (Figure 2a), implying that HPG components have been grafted from the surface of the UCNP-OH. The contents of grafted HPG calculated from the TGA curves for UCNP-*g*-HPG1 and UCNP-*g*-HPG2 are 17.5 and 38.6 wt % (Figure 2b), respectively, demonstrating that the amounts of grafted HPGs can be well tuned by adjusting R_{wt}. Because the grafted HPGs are very stable on the surface of the UCNP-*g*-HPG, the molecular weight and molecular weight polydispersity index (PDI) of grafted HPGs cannot be determined directly. On the other hand, a widely used approach under such circumstances is to investigate free polymers and then to speculate the information on the grafted polymer indirectly.[43] The molecular weight and molecular weight PDI of the free HPGs were determined by GPC (Figure 2c). The number-average molecule weight (M_n) of the free HPG increases from 5390 to 14230 with increasing R_{wt} from 8.6:1 to 25.2:1. Meanwhile, both HPG1 and HPG2 show narrow molecular weight PDIs (<1.6). These results are in accordance with the typical characteristic of a living/controlled polymerization technique.[43] The chemical structure of UCNP-*g*-HPG was further confirmed by ^{1}H NMR, as depicted in Figure 2d. The spectrum is similar to that of pure HPG[35,36] and other HPG-functionalized inorganic nanomaterials such as nanodiamond.[44] The proton resonances belonging to −OH of the HPG can be found at ca. 4.4−4.7 ppm. The proton resonances of $-CH_2-$ and −CH− of HPG are observed at 3.2−3.8 ppm.

To gain direct evidence to the formation of the HPG shell on the surface of the UCNP, the morphology of UCNP-*g*-HPG was determined by TEM. As shown in Figure 1b,c, the HPG shell on the surface of the UCNP can be clearly seen. Furthermore, the thicknesses of the HPG shell for UCNP-*g*-HPG1 and UCNP-*g*-HPG2 are 4 and 10 nm (the average sizes of UCNP-*g*-HPG1 and UCNP-*g*-HPG2 are 29 ± 7 and 34 ± 7 nm, respectively), respectively, implying that the thickness of the HPG shell can be tuned by changing R_{wt}. This fine tunability is very important because only a polymer shell with a suitable thickness is desired for bioapplications of UCNPs. To further investigate the hydrodynamic sizes of the products, DLS measurements were conducted (Figure 1d−f). The sizes of UCNP-*g*-HPG1 and UCNP-*g*-HPG2 obtained from DLS are larger than the results from TEM. This is presumably due to the fact that the HPG shells are outspread in aqueous solution but highly shrunken after drying on copper grids. In addition, the UCNP-OH sample shows aggregation with a relatively wide PDI. After polymerization, the size of the PDI of the product decreases obviously with increasing HPG content, suggesting that the introduction of a hydrophilic HPG shell is beneficial to improving the water dispersibility.

Optical Properties. Benefiting from the presence of the HPG shell, the as-prepared UCNP-*g*-HPG shows excellent dispersibility not only in aqueous solution but also in polar organic solvents such as DMSO, DMF, and ethanol (Figure S2 in the SI). This robust solution dispersibility paves the way for applications of UCNP-*g*-HPG in light-emitting devices, solar cells, and bioimaging. As shown in Figure 3a, both UCNP-*g*-HPG1 and UCNP-*g*-HPG2 in aqueous solution (1 mg/mL) present high transparency under daylight and strong UL under

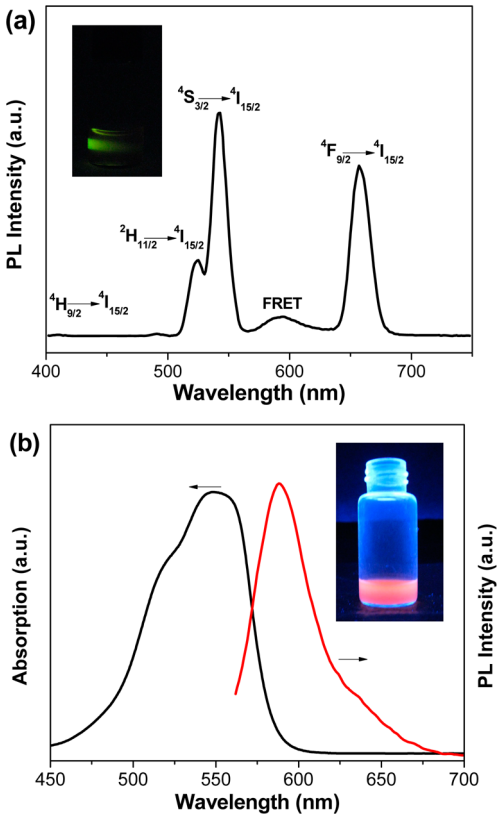

Figure 4. (a) Upconversion emission spectra (λ_{ex} = 980 nm) of UCNP-*g*-HPG-RB. Inset: photograph of the UCNP-*g*-HPG-RB in water (1 mg/mL) under 980 nm laser illumination. (b) UV−vis absorption (black line) and emission (red line) spectra of UCNP-*g*-HPG-RB in aqueous solution (λ_{ex} = 540 nm). Inset: photograph of UCNP-*g*-HPG-RB (1 mg/mL) in water under 365 nm UV-light illumination.

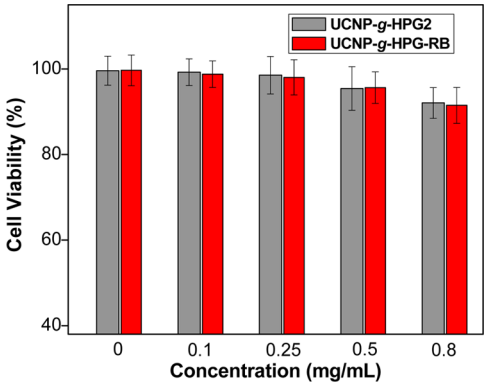

Figure 5. Cell viability of MCF-7 cells after incubation with UCNP-*g*-HPG2 and UCNP-*g*-HPG-RB at various concentrations for 24 h.

the illumination of a 980 nm laser. Correspondingly, their UL spectra were measured under excitation of a 980 nm laser. As can be seen from Figure 3a, they exhibit similar spectral character. Four typical emission peaks at 407, 524, 542, and 656 nm associated with the $^4H_{9/2} \rightarrow {}^4I_{15/2}$, $^2H_{11/2} \rightarrow {}^4I_{15/2}$, $^4S_{3/2} \rightarrow {}^4I_{15/2}$, and $^4F_{9/2} \rightarrow {}^4I_{15/2}$ transitions for Er^{3+}, respectively, can be clearly observed (also see Figure S2 in the SI).[45,46] The ratio of the UL intensity at 656 to 542 nm (I_{656}/I_{542}) is ca. 0.41 for both UCNP-*g*-HPG1 and UCNP-*g*-HPG2.

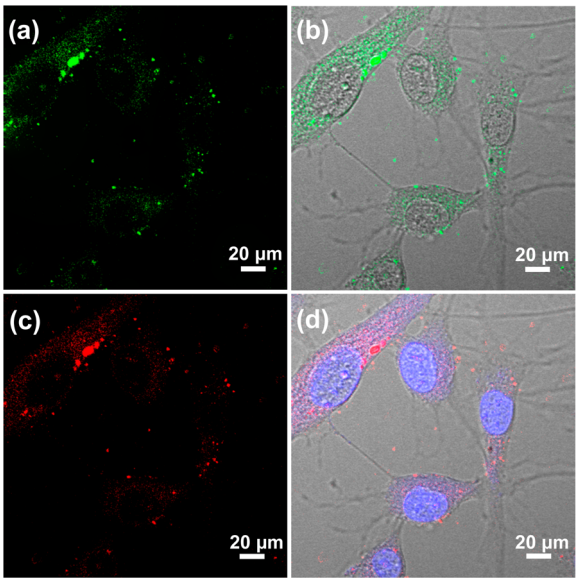

Figure 6. (a and b) UL (λ_{ex} = 980 nm) and (c and d) downconversion luminescence (λ_{ex} = 543 nm) images of MCF-7 cells upon incubation with UCNP-*g*-HPG-RB (50 μg/mL) for 2 h.

Because a complex physiological environment may disturb the optical properties of many luminescent probes, the optical properties of UCNP-*g*-HPG in aqueous media were examined under diverse conditions. UCNP-*g*-HPG2 was chosen as the representative. First, the effect of the pH on the UL change of UCNP-*g*-HPG2 is studied (Figure 3b). Less than 5% variation in the emission intensity is detected when the pH is changed from 3 to 11, implying the stable UL of UCNP-*g*-HPG2 in both acidic and basic solutions. This compares favorably to semiconductor quantum dots, which show obvious fluorescence quenching under acidic or basic conditions.[47] UCNP-*g*-HPG2 also shows a high ionic resistance performance. No obvious spectral change is detected even when the concentration of NaCl is up to 2.0 M (Figure 3c). In addition, the UL stability of UCNP-*g*-HPG2 is also investigated in the presence of bovine serum albumin (BSA), a typical protein that has been widely reported to interact with fluorophores in aqueous media.[48] To our delight, UCNP-*g*-HPG2 exhibits almost no UL change to BSA (Figure 3d). The excellent UL stability of UCNP-*g*-HPG2 can be attributed to its unique composition. The relatively stable UCNP core associated with a neutral HPG shell can effectively minimize interferences from the pH change, ionic strength variation, and protein interaction. As can be seen in Figure S3 in the SI, the apparent ζ potential value of UCNP-*g*-HPG2 is very close to zero (−0.09 mV) compared with the negatively charged UCNP-OH (−7.22 mV).

Postfunctionalization Studies. Because a variety of targeting drugs or functional molecules are required to bind with luminescent probes in practical biological applications, it is essential for luminescent agents to have multiple reactive functional groups. Fortunately, the as-prepared UCNP-*g*-HPG possesses numerous hydroxyl groups and thus offers a good platform for further conjugation with desired molecules.[49,50] To demonstrate the postmodification of UCNP-*g*-HPG, fluorescent dye RhB was chosen as a representative molecule to couple with the partial hydroxyl groups of UCNP-*g*-HPG2 (Scheme 1). The reaction process was monitored by FTIR spectra, as depicted in Figure S4 in the SI. Compared with UCNP-*g*-HPG2, the resulting UCNP-*g*-HPG-RB presents a

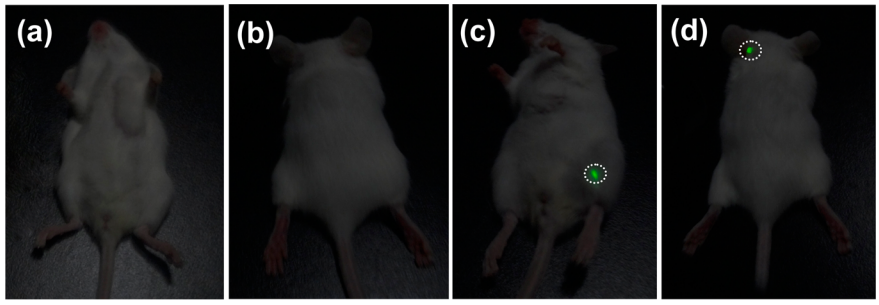

Figure 7. Digital photographs of a Kunming mouse after subcutaneous injection of 100 μL of saline (a and b) and UCNP-*g*-HPG-RB (50 μg/mL; c and d) at the leg (a and c) and bottom of the ear (b and d) regions under 980 nm laser illumination.

new peak at 1734 cm^{-1} corresponding to the O−C═O stretching, demonstrating successful reaction with RhB. The optical properties of UCNP-*g*-HPG-RB in aqueous solution were studied as shown in Figure 4. It still exhibits strong UC under excitation of a 980 nm laser (Figure 4a), indicating that UCNP-*g*-HPG2 possesses stable UC against chemical modification. In addition, the apparent ζ potential value (Figure S3 in the SI) and hydrodynamic radius distribution (Figure S5 in the SI) of UCNP-*g*-HPG-RB are similar to those of UCNP-*g*-HPG2. However, I_{656}/I_{542} of UCNP-*g*-HPG-RB is 0.74, which is much higher than that of UCNP-*g*-HPG2 (ca. 0.41). Meanwhile, a new emission peak at 588 nm assigned to the characteristic emission peak of RhB appears in the spectrum. These variations of the UL spectrum compared with those of the UCNP-*g*-HPG samples are attributed to the presence of fluorescence resonance energy transfer (FRET).[51] On the one hand, the UCNP core works as a donor in this system. Part of the emission light at the UL peak of 542 nm is absorbed by RhB because RhB exhibits strong a absorption peak at around 550 nm (Figure 4b). On the other hand, the RhB acceptor can emit fluorescence at 588 nm after absorbing light derived from UL of the UCNP. It is worth noting that FRET is strongly dependent on the distance between the donor and acceptor.[51] It is possible to deduce that the UCNP-*g*-HPG samples are promising for sensing applications by constructing a specific FRET system on the basis of its multiple hydroxyl groups and controllable shell thickness. Moreover, UCNP-*g*-HPG-RB also exhibits intensive downconversion luminescence because of the presence of the RhB moiety (Figure 4b). A dual-modal luminescent nanohybrid is pursued for advanced bioimaging applications.[52] Therefore, the grafted HPG not only improves the water dispersibility of UCNP but also serves as a versatile platform for further modification to yield new materials with desirable properties.

Preliminary Biological Evaluation. Because low toxicity is crucial for bioapplications, the cytotoxicities of UCNP-*g*-HPG2 and UCNP-*g*-HPG-RB were evaluated for MCF-7 breast cancer cells by using standard MTT cell-viability assay. Figure 5 shows the cell viability results after incubation with a sample solution at various concentrations for 24 h. The cell viabilities are close to 100% at concentrations of 0.1−0.25 mg/mL and remain over 90% at a concentration of 0.8 mg/mL within 24 h for both UCNP-*g*-HPG2 and UCNP-*g*-HPG-RB, suggesting very low cytotoxicity of the UCNP-*g*-HPG samples. The good biocompatibility of UCNP-*g*-HPG may benefit from the presence of a biocompatible HPG shell.[53,54]

On the basis of its dual-modal luminescence performance and low cytotoxicity, the application of UCNP-*g*-HPG-RB in cell imaging was studied by a confocal laser scanning microscope equipped with a 980 nm NIR laser. MCF-7 cells were incubated in a culture medium with a UCNP-*g*-HPG-RB solution for 2 h. It is noted that the concentration of UCNP-*g*-HPG-RB used for bioimaging (50 μg/mL) is much lower than that for MTT assay. Figure 6 shows the CLSM images of cells after incubation with UCNP-*g*-HPG-RB for 2 h. It can be clearly seen that the cells exhibited bright-green UL under an excitation of 980 nm (Figure 6a,b), confirming that UCNP-*g*-HPG-RB is efficiently internalized by MCF-7 cells. This result also indicates that UL of UCNP-*g*-HPG-RB is strong enough for cell imaging. In contrast, no UL can be observed for the cells without incubation of UCNP-*g*-HPG-RB (Figure S6 in the SI). In addition, the content of Y^{3+} uptake by MCF-7 cells was determined by inductively coupled plasma mass spectrometry (Agilent 7500cx) after treatment of the incubated cells with aqua regia. It is calculated that about 82−87% of UCNP-*g*-HPG-RB was internalized by the MCF-7 cells. When the cells were imaged under an excitation of 543 nm (Figure 6c,d), strong red fluorescence derived from the RhB moiety is observed in the cytoplasm around the nuclei (blue, stained by DAPI), further demonstrating the feasibility of using UCNP-*g*-HPG-RB as an imaging agent. In addition, we also studied the use of UCNP-*g*-HPG-RB for imaging of deep tissue preliminarily. A total of 100 μL of a UCNP-*g*-HPG-RB solution (50 μg/mL) was injected respectively at the leg and bottom of the ear regions of anaesthetized Kunming mice. In contrast to saline without UL, obvious UL could be seen at the injection positions with the naked eye even when the depths of injection reached 4 mm (Figure 7). In addition, this result is highly reproducible. On the basis of the above studies, we believe that the UCNP-*g*-HPG nanohybrid holds promise for bioimaging applications.

4. CONCLUSION

In summary, we have demonstrated an effective approach to fabricating a robust UCNP-*g*-HPG nanohybrid composed of a $NaYF_4$:Yb/Er core and a tunable HPG shell via a surface-initiated ROP technique. The unique structure and composition endow UCNP-*g*-HPG with desired features for bioimaging application such as good water dispersibility, strong and stable UL, low cytotoxicity, and favorable light penetration depth. Furthermore, the numerous hydroxyl groups of UCNP-*g*-HPG allow for further functionalization, as exemplified by the synthesis of a dual-modal luminescent UCNP-*g*-HPG-RB nanohybrid. The concept of grafting HPG can also be extended to other UCNPs to yield advanced upconverting nanohybrids with desirable physicochemical properties for various imaging, sensing, and drug-delivery applications.

■ ASSOCIATED CONTENT

Supporting Information

XRD curve of UCNP-OH, upconversion performance of UCNP-*g*-HPG2 in various organic solvents, apparent ζ potential of UCNP-OH, UCNP-*g*-HPG1, UCNP-*g*-HPG2, and UCNP-*g*-HPG-RB, FTIR spectrum and hydrodynamic radius distribution of UCNP-*g*-HPG-RB, and control confocal image of MCF-7 cells under an excitation of 980 nm. This material is available free of charge via the Internet at http://pubs.acs.org.

■ AUTHOR INFORMATION

Corresponding Author

*E-mail: zhouli@glut.edu.cn.

Notes

The authors declare no competing financial interest.

■ ACKNOWLEDGMENTS

The authors appreciate financial support from the National Natural Science Foundation of China (Grants 51103028 and 21364003), Guangxi Natural Science Foundation (Grants 2012GXNSFBA053152 and 2013GXNSFDA019008), Innovation Project of Guangxi Graduate Education (YCSZ2014150), and Guangxi Funds for Specially-appointed Expert and Guangxi Small Highland Innovation Team of Talents in Colleges and Universities.

■ REFERENCES

(1) Wang, F.; Han, Y.; Lim, C. S.; Lu, Y.; Wang, J.; Xu, J.; Chen, H.; Zhang, C.; Hong, M.; Liu, X. Simultaneous Phase and Size Control of Upconversion Nanocrystals Through Lanthanide Doping. *Nature* **2010**, *463*, 1061−1065.

(2) Wang, F.; Liu, X. Recent Advances in the Chemistry of Lanthanide-Doped Upconversion Nanocrystals. *Chem. Soc. Rev.* **2009**, *38*, 976−989.

(3) Haase, M.; Schäfer, H. Upconverting Nanoparticles. *Angew. Chem., Int. Ed.* **2011**, *50*, 5808−5829.

(4) Cheng, L.; Wang, C.; Liu, Z. Upconversion Nanoparticles and Their Composite Nanostructures for Biomedical Imaging and Cancer Therapy. *Nanoscale* **2013**, *5*, 23−37.

(5) Chatterjee, D. K.; Gnanasammandhan, M. K.; Zhang, Y. Small Upconverting Fluorescent Nanoparticles for Biomedical Applications. *Small* **2010**, *6*, 2781−2795.

(6) Zhou, J.; Liu, Z.; Li, F. Upconversion Nanophosphors for Small-Animal Imaging. *Chem. Soc. Rev.* **2012**, *41*, 1323−1349.

(7) Gnach, A.; Bednarkiewicz, A. Lanthanide-Doped Up-Converting Nanoparticles: Merits and Challenges. *Nano Today* **2012**, *7*, 532−563.

(8) Wang, M.; Abbineni, G.; Clevenger, A.; Mao, C.; Xu, S. Upconversion Nanoparticles: Synthesis, Surface Modification and Biological Applications. *Nanomed.: Nanotechnol., Biol. Med.* **2011**, *7*, 710−729.

(9) Liu, Y.; Tu, D.; Zhu, H.; Chen, X. Lanthanide-Doped Luminescent Nanoprobes: Controlled Synthesis, Optical Spectroscopy, and Bioapplications. *Chem. Soc. Rev.* **2013**, *42*, 6924−6958.

(10) Nyk, M.; Kumar, R.; Ohulchanskyy, T. Y.; Bergey, E. J.; Prasad, P. N. High Contrast in Vitro and in Vivo Photoluminescence Bioimaging Using Near Infrared to Near Infrared Up-Conversion in Tm^{3+} and Yb^{3+} Doped Fluoride Nanophosphors. *Nano Lett.* **2008**, *8*, 3834−3838.

(11) Naccache, R.; Vetrone, F.; Mahalingam, V.; Cuccia, L. A.; Capobianco, J. A. Controlled Synthesis and Water Dispersibility of Hexagonal Phase $NaGdF_4$:Ho^{3+}/Yb^{3+} Nanoparticles. *Chem. Mater.* **2009**, *21*, 717−723.

(12) Wang, C.; Tao, H.; Liang, C.; Liu, Z. Near-Infrared Light Induced in Vivo Photodynamic Therapy of Cancer Based on Upconversion Nanoparticles. *Biomaterials* **2011**, *32*, 6145−6154.

(13) Chen, Z.; Chen, H.; Hu, H.; Yu, M.; Li, F.; Zhang, Q.; Zhou, Z.; Yi, T.; Huang, C. Versatile Synthesis Strategy for Carboxylic Acid−Functionalized Upconverting Nanophosphors as Biological Labels. *J. Am. Chem. Soc.* **2008**, *130*, 3023−3029.

(14) Budijono, S. J.; Shan, J.; Yao, N.; Miura, Y.; Hoye, T.; Austin, R. H.; Ju, Y.; Prud'homme, R. K. Synthesis of Stable Block-Copolymer-Protected $NaYF_4$:Yb^{3+}, Er^{3+} Up-Converting Phosphor Nanoparticles. *Chem. Mater.* **2010**, *22*, 311−318.

(15) Tian, G.; Gu, Z.; Zhou, L.; Yin, W.; Liu, X.; Yan, L.; Jin, S.; Ren, W.; Xing, G.; Li, S.; Zhao, Y. Mn^{2+} Dopant-Controlled Synthesis of $NaYF_4$:Yb/Er Upconversion Nanoparticles for in vivo Imaging and Drug Delivery. *Adv. Mater.* **2012**, *24*, 1226−1231.

(16) Cui, S.; Chen, H.; Zhu, H.; Tian, J.; Chi, X.; Qian, Z.; Achilefuc, S.; Gu, Y. Amphiphilic Chitosan Modified Upconversion Nanoparticles for in Vivo Photodynamic Therapy Induced by Near-Infrared Light. *J. Mater. Chem.* **2012**, *22*, 4861−4873.

(17) Liu, Z. Y.; Yi, G. S.; Zhang, H. T.; Ding, J.; Zhang, Y. W.; Xue, J. M. Monodisperse Silica Nanoparticles Encapsulating Upconversion Fluorescent and Superparamagnetic Nanocrystals. *Chem. Commun.* **2008**, 694−696.

(18) Hu, H.; Xiong, L.; Zhou, J.; Li, F.; Cao, T.; Huang, C. Multimodal-Luminescence Core−Shell Nanocomposites for Targeted Imaging of Tumor Cells. *Chem.−Eur. J.* **2009**, *15*, 3577−3584.

(19) Liu, Q. A.; Li, C. Y.; Yang, T. S.; Yi, T.; Li, F. Y. "Drawing" Upconversion Nanophosphors into Water Through Host−Guest Interaction. *Chem. Commun.* **2010**, *46*, 5551−5553.

(20) Wang, L.; Yan, R.; Huo, Z.; Wang, L.; Zeng, J.; Bao, J.; Wang, X.; Peng, Q.; Li, Y. Fluorescence Resonant Energy Transfer Biosensor Based on Upconversion-Luminescent Nanoparticles. *Angew. Chem., Int. Ed.* **2005**, *44*, 6054−6057.

(21) Wang, F.; Chatterjee, D. K.; Li, Z. Q.; Zhang, Y.; Fan, X. P.; Wang, M. Q. Synthesis of Polyethylenimine/$NaYF_4$ Nanoparticles with Upconversion Fluorescenc. *Nanotechnology* **2006**, *17*, 5786−5791.

(22) Li, Z. Q.; Zhang, Y. Monodisperse Silica-Coated Polyvinylpyrrolidone/$NaYF_4$ Nanocrystals with Multicolor Upconversion Fluorescence Emission. *Angew. Chem., Int. Ed.* **2006**, *45*, 7732−7735.

(23) Wang, M.; Mi, C. C.; Liu, J. L.; Wu, X. L.; Zhang, Y. X.; Hou, W.; Li, F.; Xu, S. K. One-Step Synthesis and Characterization of Water-Soluble $NaYF_4$:Yb,Er/Polymer Nanoparticles with Efficient Up-Conversion Fluorescence. *J. Alloys Compd.* **2009**, *485*, L24−L27.

(24) Jin, J.; Gu, Y. J.; Man, C. W. Y.; Cheng, J.; Xu, Z.; Zhang, Y.; Wang, H.; Lee, V. H. Y.; Cheng, S. H.; Wong, W. T. Polymer-Coated $NaYF_4$:Yb^{3+}, Er^{3+} Upconversion Nanoparticles for Charge-Dependent Cellular Imaging. *ACS Nano* **2011**, *5*, 7838−7847.

(25) Xiong, L. Q.; Chen, Z. G.; Yu, M. X.; Li, F. Y.; Liu, C.; Huang, C. H. Synthesis, Characterization, and in Vivo Targeted Imaging of Amine-Functionalized Rare-Earth Up-Converting Nanophosphors. *Biomaterials* **2009**, *30*, 5592−5600.

(26) Zhou, J.; Yao, L. M.; Li, C. Y.; Li, F. Y. A Versatile Fabrication of Upconversion Nanophosphors with Functional-Surface Tunable Ligands. *J. Mater. Chem.* **2010**, *20*, 8078−8085.

(27) Yi, G. S.; Chow, G. M. Water-Soluble $NaYF_4$:Yb,Er(Tm)/$NaYF_4$/Polymer Core/Shell/Shell Nanoparticles with Significant Enhancement of Upconversion Fluorescence. *Chem. Mater.* **2007**, *19*, 341−343.

(28) He, L.; Feng, L.; Cheng, L.; Liu, Y.; Li, Z.; Peng, R.; Li, Y.; Guo, L.; Liu, Z. Multilayer Dual-Polymer-Coated Upconversion Nanoparticles for Multimodal Imaging and Serum-Enhanced Gene Delivery. *ACS Appl. Mater. Interfaces* **2013**, *5*, 10381−10388.

(29) Decher, G. Fuzzy Nanoassemblies: Toward Layered Polymeric Multicomposites. *Science* **1997**, *277*, 1232−1237.

(30) Kong, H.; Gao, C.; Yan, D. Controlled Functionalization of Multiwalled Carbon Nanotubes by in Situ Atom Transfer Radical Polymerization. *J. Am. Chem. Soc.* **2004**, *126*, 412−413.

(31) Duan, H.; Kuang, M.; Wang, D.; Kurth, D. G.; Möhwald, H. Colloidally Stable Amphibious Nanocrystals Derived from Poly{[2-(dimethylamino)ethyl] Methacrylate} Capping. *Angew. Chem., Int. Ed.* **2005**, *44*, 1717−1720.
(32) Ye, X.; Collins, J. E.; Kang, Y.; Chen, J.; Chen, D. T. N.; Yodh, A. G.; Murray, C. B. Morphologically Controlled Synthesis of Colloidal Upconversion Nanophosphors and Their shape-Directed Self-Assembly. *Proc. Natl. Acad. Sci. U. S. A.* **2010**, *107*, 22430−22435.
(33) Wang, M.; Mi, C. C.; Wang, W. X.; Liu, C. H.; Wu, Y. F.; Xu, Z. R.; Mao, C. B.; Xu, S. K. Immunolabeling and NIR-Excited Fluorescent Imaging of HeLa Cells by Using $NaYF_4$:Yb,Er Upconversion Nanoparticles. *ACS Nano* **2009**, *3*, 1580−1586.
(34) Jalil, R. A.; Zhang, Y. Biocompatibility of Silica Coated $NaYF_4$ Upconversion Fluorescent Nanocrystals. *Biomaterials* **2008**, *29*, 4122−4128.
(35) Krämer, K. W.; Biner, D.; Frei, G.; Güdel, H. U.; Hehlen, M. P.; Lüthi, S. R. Hexagonal Sodium Yttrium Fluoride Based Green and Blue Emitting Upconversion Phosphors. *Chem. Mater.* **2004**, *16*, 1244−1251.
(36) Sunder, A.; Hanselmann, R.; Frey, H.; Mülhaupt, R. Controlled Synthesis of Hyperbranched Polyglycerols by Ring-Opening Multibranching Polymerization. *Macromolecules* **1999**, *32*, 4240−4246.
(37) Kainthan, R. K.; Muliawan, E. B.; Hatzikiriakos, S. G.; Brooks, D. E. Synthesis, Characterization, and Viscoelastic Properties of High Molecular Weight Hyperbranched Polyglycerols. *Macromolecules* **2006**, *39*, 7708−7717.
(38) Wilms, D.; Stiriba, S. E.; Frey, H. Hyperbranched Polyglycerols: From the Controlled Synthesis of Biocompatible Polyether Polyols to Multipurpose Applications. *Acc. Chem. Res.* **2010**, *43*, 129−141.
(39) Calderón, M.; Quadir, M. A.; Sharma, S. K.; Haag, R. Dendritic Polyglycerols for Biomedical Applications. *Adv. Mater.* **2010**, *22*, 190−218.
(40) Kainthan, R. K.; Hester, S. R.; Levina, E.; Devine, D. V.; Brooks, D. E. In Vitro Biological Evaluation of High Molecular Weight Hyperbranched Polyglycerols. *Biomaterials* **2007**, *28*, 4581−4590.
(41) He, B.; Zhou, L.; Huang, J. One-Step Synthesis of Water-Dispersible Hydroxyl-Functionalized $NaYF_4$:Yb/Er Upconversion Nanoparticles. *Mater. Lett.* **2014**, *117*, 142−145.
(42) Dyck, N. C.; van Veggel, F. C. J. M.; Demopoulos, G. P. Size-Dependent Maximization of Upconversion Efficiency of Citrate-Stabilized β-Phase $NaYF_4$:Yb^{3+},Er^{3+} Crystals via Annealing. *ACS Appl. Mater. Interfaces* **2013**, *5*, 11661−11667.
(43) Gao, C.; Muthukrishnan, S.; Li, W.; Yuan, J.; Xu, Y.; Müller, A. H. E. Linear and Hyperbranched Glycopolymer-Functionalized Carbon Nanotubes: Synthesis, Kinetics, and Characterization. *Macromolecules* **2007**, *40*, 1803−1815.
(44) Zhao, L.; Takimoto, T.; Ito, M.; Kitagawa, N.; Kimura, T.; Komatsu, N. Chromatographic Separation of Highly Soluble Diamond Nanoparticles Prepared by Polyglycerol Grafting. *Angew. Chem., Int. Ed.* **2011**, *50*, 1388−1392.
(45) Johnson, N. J. J.; Sangeetha, N. M.; Boyer, J. C.; van Veggel, F. C. J. M. Facile Ligand-Exchange with Polyvinylpyrrolidone and Subsequent Silica Coating of Hydrophobic Upconverting β-$NaYF_4$:Yb^{3+}/Er^{3+} Nanoparticles. *Nanoscale* **2010**, *2*, 771−777.
(46) Wang, F.; Liu, X. Upconversion Multicolor Fine-Tuning: Visible to Near-Infrared Emission from Lanthanide-Doped $NaYF_4$ Nanoparticles. *J. Am. Chem. Soc.* **2008**, *130*, 5642−5643.
(47) Liu, Y. S.; Sun, Y.; Vernier, P. T.; Liang, C. H.; Chong, S. Y. C.; Gundersen, M. A. pH-Sensitive Photoluminescence of CdSe/ZnSe/ZnS Quantum Dots in Human Ovarian Cancer Cells. *J. Phys. Chem. C* **2007**, *111*, 2872−2878.
(48) Pu, K. Y.; Liu, B. Fluorescence Turn-on Responses of Anionic and Cationic Conjugated Polymers toward Proteins: Effect of Electrostatic and Hydrophobic Interactions. *J. Phys. Chem. B* **2010**, *114*, 3077−3084.
(49) Zhou, L.; Gao, C.; Hu, X.; Xu, W. General Avenue to Multifunctional Aqueous Nanocrystals Stabilized by Hyperbranched Polyglycerol. *Chem. Mater.* **2011**, *23*, 1461−1470.
(50) Zhou, L.; Geng, J.; Wang, G.; Liu, J.; Liu, B. A Water-Soluble Conjugated Polymer Brush with Multihydroxy Dendritic Side Chains. *Polym. Chem.* **2013**, *4*, 5243−5251.
(51) Wang, Y.; Liu, K.; Liu, X.; Dohnalová, K.; Gregorkiewicz, T.; Kong, X.; Aalders, M. C. G.; Buma, W. J.; Zhang, H. Critical Shell Thickness of Core/Shell Upconversion Luminescence Nanoplatform for FRET Application. *J. Phys. Chem. Lett.* **2011**, *2*, 2083−2088.
(52) Liu, Y.; Tu, D.; Zhu, H.; Li, R.; Luo, W.; Chen, X. A Strategy to Achieve Efficient Dual-Mode Luminescence of Eu^{3+} in Lanthanides Doped Multifunctional $NaGdF_4$ Nanocrystals. *Adv. Mater.* **2010**, *22*, 3266−3271.
(53) Yu, X.; Liu, Z.; Janzen, J.; Chafeeva, I.; Horte, S.; Chen, W.; Kainthan, R. K.; Kizhakkedathu, J. N.; Brooks, D. E. Polyvalent Choline Phosphate as a Universal Biomembrane Adhesive. *Nat. Mater.* **2012**, *11*, 468−476.
(54) Zhou, L.; Geng, J.; Wang, G.; Liu, J.; Liu, B. Facile Synthesis of Stable and Water-Dispersible Multihydroxy Conjugated Polymer Nanoparticles with Tunable Size by Dendritic Cross-Linking. *ACS Macro Lett.* **2012**, *1*, 927−932.